

Article

Synthesis, Photophysical, and Computational Studies of a Bridged Ir^{III}-Pt^{II} Heterodimetallic Complex

Si-Hai Wu ^{1,*}, Dian-Xue Ma ², Zhong-Liang Gong ², Junjie Ma ¹, Jiang-Yang Shao ^{2,*}, Rong Yang ¹ and Yu-Wu Zhong ^{2,3,*}

¹ School of Medicine, Huaqiao University, Quanzhou 362021, China; majunjie3612@hqu.edu.cn (J.M.); yrr4924@163.com (R.Y.)

² Beijing National Laboratory for Molecular Sciences, CAS Key Laboratory of Photochemistry, CAS Research/Education Center for Excellence in Molecular Sciences, Institute of Chemistry, Chinese Academy of Sciences, Beijing 100190, China; mdx1997520@iccas.ac.cn (D.-X.M.); gongzhongliang@iccas.ac.cn (Z.-L.G.)

³ School of Chemical Sciences, University of Chinese Academy of Sciences, Beijing 100049, China

* Correspondence: wusihai@hqu.edu.cn (S.-H.W.); shaojiangyang@iccas.ac.cn (J.-Y.S.); zhongyuwu@iccas.ac.cn (Y.-W.Z.)

Abstract: An Ir^{III}-Pt^{II} heterodimetallic complex [(ppy)₂Ir(dapz)PtCl₂]Cl (**4**), together with the corresponding monometallic complexes [(dapz)PtCl₂] (**2**) and [(ppy)₂Ir(dapz)]Cl (**3**) was designed and prepared, where dapz is 2,5-di(*N*-methyl-*N'*-(pyrid-2-yl)amino)pyrazine and ppy is 2-phenylpyridine, respectively. Single-crystal X-ray analysis was carried out for complex **4**, displaying the intermolecular Pt···Pt and aromatic plane···plane distances of 3.839 and 3.886 Å, respectively. The monometallic complex **2** exhibits a single emission maximum at 432 nm with a shorter excited-state lifetime (τ) of 6 ns, while complex **3** exhibits an emission band at 454 nm with a longer excited-state lifetime of 135 ns in CH₃CN (N₂-saturated) under ambient conditions. In contrast, the heterodimetallic complex **4** displays intriguing excitation wavelength-dependent dual singlet and triplet emissions. Theoretical calculations of the electronic structures and absorption spectra of these complexes were carried out to assist the interpretation of these experimental findings.

Keywords: bridging ligands; transition metal complexes; dual emissions; iridium; platinum



Citation: Wu, S.-H.; Ma, D.-X.; Gong, Z.-L.; Ma, J.; Shao, J.-Y.; Yang, R.; Zhong, Y.-W. Synthesis, Photophysical, and Computational Studies of a Bridged Ir^{III}-Pt^{II} Heterodimetallic Complex. *Crystals* **2021**, *11*, 236. <https://doi.org/10.3390/cryst11030236>

Academic Editors:

Jesús Sanmartín-Matalobos and Yulia V. Nelyubina

Received: 20 January 2021

Accepted: 24 February 2021

Published: 26 February 2021

Publisher's Note: MDPI stays neutral with regard to jurisdictional claims in published maps and institutional affiliations.



Copyright: © 2021 by the authors. Licensee MDPI, Basel, Switzerland. This article is an open access article distributed under the terms and conditions of the Creative Commons Attribution (CC BY) license (<https://creativecommons.org/licenses/by/4.0/>).

1. Introduction

Emissive transition metal complexes (TMCs) with dual or multiband emissions have attracted much attention because of their intriguing luminescence properties [1,2]. A number of dual-emissive mononuclear TMCs have been developed including ruthenium [3–7], iridium [8–10], platinum [11], and other metal complexes [12–14]. Due to the presence of two or multiple distinct emission bands, these kinds of materials have been widely used in the ratiometric sensing and imaging of metal ions [15], O₂ [16–20], and biomacromolecules (protein and DNA) [21–23], with improved sensing accuracy and reliability.

One strategy to construct dual-emissive TMCs is by tuning the ligand electronic structures of mononuclear complexes such as introducing additional organic luminophores [17,18,24,25] or new ligand-localized charge-transfer excited states [19,26,27]. Another strategy is the synthesis of dinuclear or multinuclear bridged complexes with the same or different metal ions, which may exhibit interesting photophysical properties by tuning the electron/energy transfer among individual metal components [28–30]. Examples of dual-emissive dinuclear TMCs based on ruthenium [31] and platinum [32,33] complexes have been documented recently, stimulating the design and synthesis of new bridged complexes with intriguing emission properties.

In a previous work, we reported a bis-bidentate ligand dapz (dapz = 2,5-di(*N*-methyl-*N'*-(pyrid-2-yl)amino)pyrazine; Figure 1) with a larger bite angle and its application in

the synthesis of a dual-emissive mononuclear ruthenium complex [34]. To extend our research interest in the development of dual-emissive TMCs, an Ir^{III}-Pt^{II} heterodimetallic complex [(ppy)₂Ir(dapz)PtCl₂]Cl (4) and the corresponding monometallic complexes [(ppy)₂Ir(dapz)]Cl (3) and [(dapz)PtCl₂] (2) were designed and prepared. The photophysical properties of these complexes are presented herein. Moreover, density functional theory (DFT) and time-dependent DFT (TDDFT) calculations were performed and are discussed.

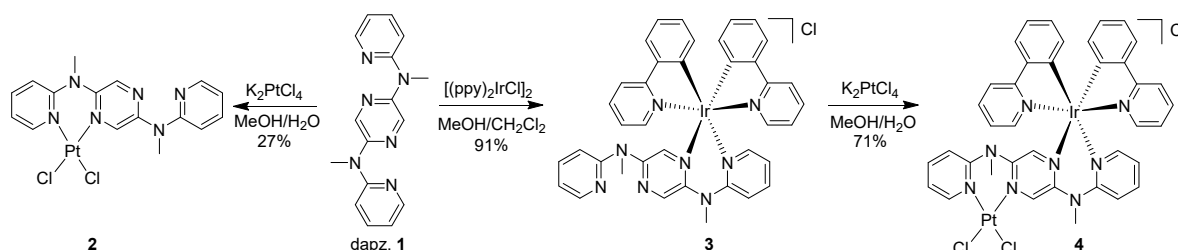


Figure 1. Synthesis of complexes 2–4.

2. Experimental Section

2.1. Spectroscopic Analysis

A TU-1810DSPC spectrometer of Beijing Purkinje General Instrument Co. Ltd. (Beijing, China) was used to measure the absorption spectra at ambient conditions. A F-380 spectrofluorometer of Tianjin Gangdong Sci. & Tech. Development Co. Ltd. (Tianjin, China) was used to measure the emission spectra. Samples for absorption and emission measurements were prepared within quartz cuvettes of a 1 cm path length. Luminescence quantum yields were calculated by using quinine sulfate in 1.0 M aq H₂SO₄ ($\Phi = 55\%$) as the standard. The uncertainty was about $\pm 10\%$ or better. A Bruker Avance 300 or 400 MHz spectrometer (Bruker, Billerica, MA, USA) was used to obtain the ¹H and ¹³C NMR spectra. A Waters MALDI micro MX mass spectrometer (Bruker, Karlsruhe, BW, Germany) was used to record the MALDI-TOF positive ion data in a reflection mode. A Flash EA 1112 or Carlo Erba 1106 analyzer (Thermo Fisher Scientific, Waltham, MA, USA) was used to record elemental analysis results. Thermal analysis was carried out using a PerkinElmer TGA 8000 under nitrogen (PerkinElmer Inc., Waltham, MA, USA).

2.2. Emission Lifetime Analysis

The luminescence decays were analyzed on a Hamamatsu Quantaaurus-Tau Fluorescence lifetime spectrometer C11367 (Hamamatsu Photonics K.K., Shizuoka, Japan) and a nanosecond flash photolysis setup (Edinburgh FLS920 spectrometer) equipped with a picosecond pulsed diode laser (Edinburgh Instruments, Edinburgh, UK).

2.3. DFT and TDDFT Calculations

Gaussian 09 package (revision 09, Gaussian Inc., Wallingford, CT, USA) and the B3LYP exchange correlation functional were used to carry out the DFT calculations. The electronic structures were optimized with the LANL2DZ basis set for Ir, Pt, and 6-31G* for other atoms. All calculations were performed taking into account the solvation effects in CH₃CN. No symmetry constraints were used for all of the calculations. In order to ensure the optimized geometries to be local minima, frequency calculations were carried out at the same level of theory. All orbitals were computed by setting an isovalue of 0.02 e bohr⁻³. With the same level of theory, the DFT-optimized structures were used for the subsequent TDDFT calculations.

2.4. X-ray Crystallography

A Rigaku Saturn 724 diffractometer on a rotating anode (Mo K α radiation, 0.71073 Å) was used to collect the X-ray diffraction data at 173 K. The structure solution and

refinement were performed on SHELXS-97 and Olex2 software (version Olex2.refine, Durham University, UK). Olex2 software was used to generate the structure graphics shown in Figure 2.

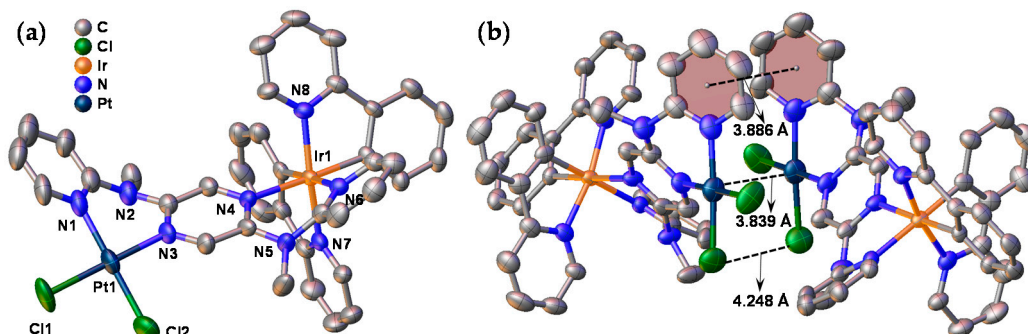


Figure 2. (a) ORTEP diagram of the single-crystal X-ray structure and (b) crystal packing of complex 4 with 50% probability of the thermal ellipsoids. For the reason of clarity, H atoms and solvents were omitted. The intermolecular aromatic plane...plane, Pt...Pt and Cl...Cl distances are indicated in (b).

2.5. Synthesis

All reagents were purchased from commercial resources and used as received. Standard Schlenk techniques were employed to run all reactions under N_2 .

2.5.1. [(dapz)PtCl₂] (2)

A suspension of K_2PtCl_4 (41.5 mg, 0.1 mmol) and dapz (1) (29.2 mg, 0.1 mmol) [34] in MeOH/ H_2O (5 mL/5 mL) was refluxed for 12 h. After cooling to room temperature, the solvent was evaporated under reduced pressure. Silica gel chromatography (eluent: CH_2Cl_2 /MeOH = 100/5) was used to purify the crude product to provide 15 mg of complex 2 as a yellow solid in 27% yield. 1H NMR (400 MHz, CD_2Cl_2): δ 3.59 (s, 3H), 3.66 (s, 3H), 7.04 (t, $J = 6.4$ Hz, 1H), 7.09 (t, $J = 6.8$ Hz, 1H), 7.16 (t, $J = 7.6$ Hz, 2H), 7.72 (t, $J = 8.4$ Hz, 1H), 7.91 (t, $J = 8.0$ Hz, 1H), 8.16 (s, 1H), 8.35 (d, $J = 4.8$ Hz, 1H), 9.00 (d, $J = 6.0$ Hz, 1H), 9.25 (s, 1H). MALDI-MS (m/z): 523.2 for $[M-Cl]^+$, 486.2 for $[M-2Cl-1]^2+$. Anal. Calcd. for $C_{16}H_{16}Cl_2N_6Pt \cdot H_2O$: C, 33.34; H, 3.15; N, 14.58. Found: C, 33.57; H, 3.01; N, 14.18.

2.5.2. [(ppy)₂Ir(dapz)]Cl (3)

A mixture of dapz (21 mg, 0.07 mmol) and [(ppy)₂IrCl]₂ (32 mg, 0.03 mmol) was added to the mixed solvent of 5 mL of CH_2Cl_2 and 5 mL of MeOH. The mixture was heated under reflux for 18 h. The solvent was then removed under reduced pressure. The crude product was purified by flash chromatography using silica gel (eluent: CH_2Cl_2 /MeOH = 100/8) to give 45 mg of complex 3 as a yellow solid in 91% yield. 1H NMR (400 MHz, CD_2Cl_2): δ 3.41 (s, 3H), 3.65 (s, 3H), 6.12 (d, $J = 7.6$ Hz, 1H), 6.16 (d, $J = 7.6$ Hz, 1H), 6.71 (t, $J = 7.6$ Hz, 1H), 6.80–7.00 (m, 6H), 7.18–7.24 (m, 2H), 7.54–7.59 (m, 3H), 7.64 (d, $J = 7.6$ Hz, 1H), 7.74 (d, $J = 5.2$ Hz, 1H), 7.87–7.97 (m, 7H), 8.09 (d, $J = 6.0$ Hz, 1H), 8.26 (d, $J = 6.0$ Hz, 1H), 8.59 (s, 1H). ^{13}C NMR (75 MHz, CD_3CN): δ 35.6, 40.7, 114.3, 116.6, 119.4, 120.3, 120.7, 121.0, 123.0, 123.1, 123.3, 123.6, 125.2, 125.5, 130.5, 130.7, 132.1, 132.2, 135.2, 137.4, 139.2, 140.9, 144.5, 144.6, 144.8, 148.6, 149.7, 150.3, 150.7, 151.0, 151.5, 156.4, 157.6, 167.9. MALDI-MS (m/z): 793.5 for $[M-Cl]^+$. MALDI-HRMS (m/z) calcd. for $C_{38}H_{32}N_8Ir$: 793.2375. Found: 793.2371. Anal. Calcd. for $C_{38}H_{32}ClN_8Ir \cdot 2H_2O$: C, 52.80; H, 4.20; N, 12.96. Found: C, 52.75; H, 4.24; N, 12.63.

2.5.3. [(ppy)₂Ir(dapz)PtCl₂]Cl (4)

A suspension of complex 3 (149 mg, 0.18 mmol) and K_2PtCl_4 (83 mg, 0.2 mmol) in MeOH/ H_2O (10 mL/10 mL) was refluxed under N_2 for 1 h. After removing the solvent

under reduced pressure, the crude product was purified by silica gel chromatography (eluent: $\text{CH}_2\text{Cl}_2/\text{MeOH} = 100/15$) to afford 140 mg of complex **4** as an orange solid in 71% yield. $^1\text{H NMR}$ (400 MHz, CD_3CN): δ 2.94 (s, 3H), 3.56 (s, 3H), 6.16 (d, $J = 7.6$ Hz, 1H), 6.22 (d, $J = 7.6$ Hz, 1H), 6.86 (t, $J = 7.2$ Hz, 1H), 6.94 (t, $J = 8.0$ Hz, 2H), 7.02 (q, $J = 8.4$ Hz, 2H), 7.09–7.17 (m, 3H), 7.22 (t, $J = 6.4$ Hz, 1H), 7.54–7.60 (m, 2H), 7.68 (s, 1H), 7.74 (d, $J = 7.6$ Hz, 1H), 7.81 (d, $J = 7.6$ Hz, 1H), 7.93–7.98 (m, 4H), 8.05 (d, $J = 7.6$ Hz, 1H), 8.12–8.16 (m, 2H), 8.20 (d, $J = 5.6$ Hz, 1H), 8.82 (d, $J = 5.6$ Hz, 1H), 9.22 (s, 1H). MALDI-MS (m/z): 1058.1 for $[\text{M} - \text{Cl}]^+$. MALDI-HRMS (m/z) calcd. for $\text{C}_{38}\text{H}_{32}\text{Cl}_2\text{IrN}_8\text{Pt}$: 1058.1390. Found: 1058.1406. Anal. Calcd. for $\text{C}_{38}\text{H}_{32}\text{Cl}_3\text{IrN}_8\text{Pt} \cdot 3\text{H}_2\text{O}$: C, 39.74; H, 3.34; N, 9.76. Found: C, 39.45; H, 3.16; N, 9.83.

3. Results and Discussion

3.1. Synthesis and Single Crystal X-ray Analysis

The compounds that were studied in this work are displayed in Figure 1. The bridging ligand dapz (**1**) was prepared according to the previously reported procedure [34]. The treatment of K_2PtCl_4 with **1** in a mixture of methanol and water afforded the mononuclear Pt^{II} complex **2** in 27% yield. The yield of this reaction was not optimized. However, when this reaction was performed in acetic acid [35,36] or a mixture of water and acetonitrile [37,38], no desired product could be isolated, and the reason is not clear at this stage. By the treatment of ligand **1** with the Ir^{III} dimer $[(\text{ppy})_2\text{IrCl}]_2$ ($\text{ppy} = 2\text{-phenylpyridine}$) in a mixture of methanol and dichloromethane [39], the mononuclear Ir^{III} complex **3** was isolated in a high yield of 91% after purification by flash column chromatography. When complex **3** was further treated with one equiv of K_2PtCl_4 in a mixture of methanol and water, the $\text{Ir}^{\text{III}}\text{-Pt}^{\text{II}}$ heterodimetallic complex **4** was obtained in 71% yield after flash column chromatography. All new compounds were thoroughly characterized by mass and NMR spectrometry, as well as elemental analysis. The comparison of $^1\text{H NMR}$ spectra of **1–4** is shown in Figure S1. After coordination with a $[\text{PtCl}_2]$ or $[(\text{ppy})_2\text{Ir}]$ unit, the methyl protons of ligand **1** were split into two peaks with some degree of shifts in complexes **2–4**, suggestive of the asymmetric structures of these compounds. In addition, compared to those of ligand **1**, one singlet pyrazine proton and one doublet α -pyridine proton of the platinum complexes **2** and **4** shift distinctly to the low field. HPLC analysis shows high purity of over 99% for both dapz and **4** (Figure S2). The ^1H and ^{13}C NMR spectra of new complexes are provided in the Supporting Information (Figures S3–S6). The thermogravimetric analysis indicated that complexes **3** and **4** show thermal decomposition temperatures of 178 and 281 °C at a 5% weight loss, respectively (Figure S7).

The structure of complex **4** was also confirmed by single-crystal X-ray analysis. The ORTEP and crystal packing of **4** are shown in Figure 2. Corresponding crystallographic data are summarized in Tables S1 and S2. The single crystal of **4** was obtained by the slow diffusion of diethyl ether into a solution of **4** in acetonitrile. The Ir atom adopts a distorted octahedral configuration surrounded by dapz and two ppy ligands, whereas the Pt atom possesses a square planar coordination geometry. The N–Ir–N bite angle with the dapz ligand ($85.94(14)^\circ$) is slightly larger with respect to the C–Ir–N bite angles associated with two ppy ligands ($80.44(15)$ and $80.63(16)^\circ$ respectively). The N–Pt–N bite angle with the dapz ligand ($87.95(16)^\circ$) is also larger than those of most platinum complexes with $\text{N}^{\wedge}\text{N}$ bidentate ligands, which fall in the range of $77.5(2)$ – $79.02(14)^\circ$ [40–42]. The Ir–N bond lengths with dapz (2.167(4) and 2.174(3) Å) are slightly longer than the Ir–C bond lengths with ppy (2.063(3) and 2.055(3) Å). The Pt–N bond lengths with dapz (2.007(4) and 2.032(5) Å) are similar to those of known platinum complexes [38,40–42]. As suggested by Figure 2b, the intermolecular Cl \cdots Cl distance is 4.248 Å, indicating the absence of Cl \cdots Cl interaction. The intermolecular aromatic plane \cdots plane and Pt \cdots Pt distances of complex **4** are 3.886 and 3.839 Å, respectively. The distance is slightly larger than, but close to, the Pt \cdots Pt interaction distance [43,44] and conventional π – π stacking [45]. This suggests that the intermolecular π – π and Pt \cdots Pt interactions, if present, are rather weak in the crystal of complex **4**.

3.2. DFT Calculations

In order to understand the electronic structure of these complexes, DFT calculations were performed on **2**, **3**⁺, and **4**⁺ (counteranions were not considered) with the B3LYP/LANL2DZ/6-31G*/CPCM method. Figure 3a shows the calculated energy diagram of these complexes. The frontier energy gaps of **2** and **3**⁺ were calculated to be 3.73 and 3.65 eV, respectively. Complex **4**⁺ has a calculated energy gap of 2.9 eV, which is much narrower than those of **2** and **3**⁺. This is mainly ascribed to the stabilization of the lowest unoccupied molecular orbital (LUMO) level of **4**⁺. The isodensity plots of some representative orbitals of these complexes are shown in Figure S8 (**2**), Figure S9 (**3**⁺), and Figure 3b (**4**⁺). The highest occupied molecular orbital (HOMO) of complex **2** is dominated by the ligand dapz, while the HOMO–1, HOMO–2, and HOMO–3 of **2** are associated with the platinum component (Figure S8). The LUMO of **2** has a major contribution from the central pyrazine unit of dapz and the [PtCl₂] unit and the pyridine segments of dapz make bigger contributions to the higher unoccupied orbitals. The HOMO and HOMO–1 of complex **3** are associated with the iridium component and ligand dapz, while its HOMO–2 and HOMO–3 are dominated by the iridium component (Figure S9). The LUMO of **3**⁺ is also dominated by the central pyrazine unit of dapz and its higher unoccupied orbitals are associated with ppy ligands. The HOMO, HOMO–1, and HOMO–3 of **4**⁺ are dominated by the iridium component, while its HOMO–2 has significant contributions from the ligand dapz, with little contributions from the platinum component (Figure 3b). The LUMO of **4**⁺ has the same character as those of **2** and **3**⁺, associated with the central pyrazine unit of dapz. The LUMO+1 of **4**⁺ is dominated by the [PtCl₂] unit. Other higher unoccupied orbitals of **4**⁺ are associated with the dapz and ppy ligands.

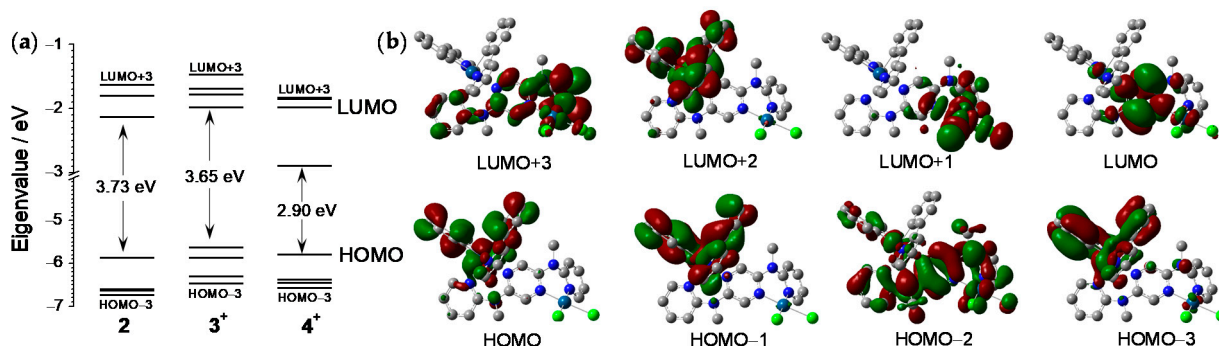


Figure 3. (a) DFT-calculated energy diagram of **2**, **3**⁺, and **4**⁺. The HOMO–LUMO gap is indicated by an arrow. (b) Isodensity plots of frontier orbitals of **4**⁺. Isovalue = 0.02 e bohr^{−3}.

3.3. Absorption Studies and TDDFT Calculations

The electronic absorption spectra of compounds **1–4** are displayed in Figure 4a. Corresponding data, including absorption maxima and molar absorption coefficients, are delineated in Table 1. Transitions in the UV region are largely caused by intraligand π – π^* excitations, while the absorption bands in the visible region are attributed to charge transfer (CT) transitions. The lower-energy side of the visible absorptions of the dimetallic complex **4** extends to the region with wavelengths longer than 500 nm, which are distinctly red-shifted with respect to that of **1–3**. This is in agreement with the above DFT calculations showing that complex **4** has the narrowest energy gap.

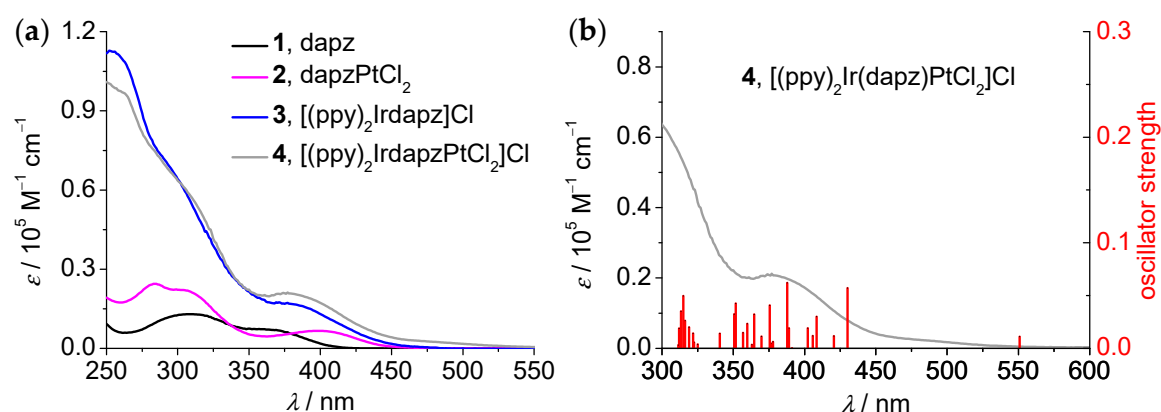


Figure 4. (a) UV/vis absorption spectra of 1–4 in acetonitrile at a concentration of 5.0×10^{-6} M. (b) Time-dependent DFT (TDDFT) results of complex 4^+ .

Table 1. Absorption and emission data of complexes 2–4 and dapz ^a.

Compound	$\lambda_{\text{abs(max)}/\text{nm}}$ ($\epsilon/10^5$ $\text{M}^{-1}\text{cm}^{-1}$)	$\lambda_{\text{em(max)}}^{\text{b}}/\text{nm}$	τ (N_2) ^c /ns	Φ^{d}
1	309 (0.13), 369 (0.07)	460	10	43%
2	284 (0.24), 305 (0.22), 402 (0.07)	432	6 (at 410 nm)	3.2%
3	252 (1.13), 303 (0.62), 370 (0.15)	454	135 (at 480 nm)	5.8%
4	264 (0.96), 317 (0.43), 377 (0.21), 491 (0.02)	420/520	8/99	1.5%

^a All spectra were measured in a 1.0 cm quartz cell (5×10^{-6} M in CH_3CN). ^b The excitation wavelength is 340 nm for 1 and 2 and 360 nm for 3 and 4, respectively. ^c The data were simulated by a mono- (1, 2), bi- (3), and triexponential (4) decay. Recorded as the average lifetime τ in the case of multiexponential decay by $\tau = [A_1(\tau_1)^2 + A_2(\tau_2)^2 + \dots + A_n(\tau_n)^2]/(A_1\tau_1 + A_2\tau_2 + \dots + A_n\tau_n)$. ^d Relative quantum yield compared to that of quinine sulfate in 1.0 M aq H_2SO_4 (55%).

In order to assist in the assignment of the electronic absorptions, the nature of the low energy transitions was investigated by TDDFT calculations. The predicted transitions of complexes 2, 3⁺, and 4⁺ are shown in Figure S10 (2 and 3⁺) and Figure 4b (4⁺). Table 2 collects major predicted transitions with the excitation energy, oscillator strength (f), dominant configuration contribution and assignment. The mononuclear platinum complex 2 shows a broad band centered at 402 nm. The TDDFT results indicate that the S_1 state ($f = 0.0648$) is responsible for this band. This state is mainly assigned to the HOMO \rightarrow LUMO excitation, with a character of intraligand charge transfer (ILCT) from the aminopyridine units to the central pyrazine unit of dapz. The mononuclear iridium complex 3 displays an absorption band centered at 370 nm. According to the TDDFT results, this band is ascribed to the metal to ligand charge transfer (MLCT) from the Ir component to ligand dapz.

Compared to those of the Ir complex 3, the absorptions of the Ir-Pt complex 4 are slightly red shifted, showing a broad band centered at 377 nm and some weak absorptions in the region 450–550 nm. The TDDFT results of 4 suggest that the Pt based MLCT transition (S_{12} excitation, $f = 0.0408$) may contribute to the relatively higher-energy absorptions of the compound. The lower-energy absorptions in the region 450–550 nm are more likely attributed to an admixture of the iridium-based MLCT, ILCT and ligand to ligand charge transfer (LLCT) transitions (S_1 , S_2 , and S_4 states with f of 0.011, 0.057, and 0.0301, respectively).

Table 2. TDDFT results of complex 2–4 ^a.

Compound	S_n	E (ev)	λ (nm)	f	Dominant Transition(s) (Percentage Contribution ^b)	Assignment ^c
2	1	3.10	399	0.0648	HOMO \rightarrow LUMO (77%)	IL _{dapz} CT
	2	3.15	394	0.0245	HOMO–1 \rightarrow LUMO + 1 (34%) HOMO–2 \rightarrow LUMO + 1 (28%)	MC
	7	3.61	343	0.033	HOMO \rightarrow LUMO + 2 (50%)	IL _{dapz} CT
	8	3.68	337	0.0217	HOMO \rightarrow LUMO + 2 (35%)	IL _{dapz} CT
	10	3.90	318	0.122	HOMO–3 \rightarrow LUMO (70%)	M _{Pt} L _{dapz} CT
3	1	2.99	415	0.0244	HOMO \rightarrow LUMO (97%)	M _{Ir} L _{dapz} CT
	2	3.14	395	0.052	HOMO \rightarrow LUMO + 1 (89%)	M _{Ir} L _{ppy} CT/L _{dapz} L _{ppy} CT
	4	3.26	381	0.0565	HOMO–1 \rightarrow LUMO (87%)	M _{Ir} L _{dapz} CT/L _{ppy} L _{dapz} CT
	5	3.52	353	0.0369	HOMO \rightarrow LUMO + 3 (85%)	M _{Ir} L _{dapz} CT/L _{ppy} L _{dapz} CT
	11	3.83	324	0.1018	HOMO–1 \rightarrow LUMO + 3 (84%)	M _{Ir} L _{dapz} CT/L _{ppy} L _{dapz} CT
4	1	2.25	551	0.011	HOMO \rightarrow LUMO (99%)	M _{Ir} L _{dapz} CT/L _{ppy} L _{dapz} CT
	2	2.88	430	0.057	HOMO–2 \rightarrow LUMO (58%) HOMO–1 \rightarrow LUMO (32%)	M _{Ir} L _{dapz} CT/IL _{dapz} CT
	4	3.04	408	0.0301	HOMO–3 \rightarrow LUMO (61%)	M _{Ir} L _{dapz} CT/L _{ppy} L _{dapz} CT
	9	3.20	388	0.062	HOMO \rightarrow LUMO+2 (91%)	MC
	12	3.30	375	0.0408	HOMO–5 \rightarrow LUMO (17%) HOMO–5 \rightarrow LUMO + 1 (19%)	M _{Ir} L _{dapz} CT/M _{Pt} L _{dapz} CT
	14	3.40	364	0.0322	HOMO–9 \rightarrow LUMO (50%)	M _{Pt} L _{dapz} CT

^a Computed at the B3LYP/LANL2DZ/6-31G*/CPCM level of theory. ^b Actual contributions [%] = (configuration coefficient)² \times 2 \times 100.

^c ppy = phenylpyridine, dapz = 2,5-di(*N*-methyl-*N'*-(pyrid-2-yl)amino)pyrazine.

3.4. Emission Spectroscopic Studies

The above complexes were further investigated regarding their emission properties. Their emission spectra are shown in Figure 5; Figure 6, and the luminescence data are provided in Table 1. The ligand dapz **1** exhibited an emission band at 460 nm with a quantum yield of 43% and a lifetime of 10 ns in nitrogen-saturated CH₃CN (Figure 5a) [34]. The mononuclear platinum complex **2** shows an emission band at 432 nm with a quantum yield of 3.2%, and a lifetime of 6 ns in nitrogen-saturated CH₃CN. The shape of the emission spectrum is independent of the excitation wavelength and the emission lifetime is independent of the emission wavelength (Figure 5b,c). These data suggest that the emission of **2** has a Pt-perturbed ¹ILCT character. The incorporation of the [PtCl₂] component into ligand dapz leads to the significant decrease of the emission quantum yield by the heavy atom effect. The mononuclear iridium complex **3** displays an emission band at 454 nm, with a quantum yield of 5.8% in CH₃CN under nitrogen-saturated conditions. As suggested by TDDFT calculations, we believe that the dapz-targeted ³MLCT transition is responsible for the observed emission at 454 nm. The excited-state lifetime was determined as 19 and 135 ns in air-equilibrated and nitrogen-saturated conditions, respectively. This is in accordance with the excited-state lifetime of the most reported mononuclear cyclometalated iridium complexes [46–48]. In addition, the emission lifetime of **3** is also basically independent of the decay wavelength (Figure 5e). These results suggest that the emissions of **2** and **3** were originated from a single singlet and triplet excited state, respectively.

In contrast, the heterodimetallic complex **4** exhibits dual emissive behavior dependent on the excitation wavelength (Figure 6). Upon excitation at 350 nm, complex **4** shows a major emission band at about 420 nm and a shoulder emission band at around 520 nm with a total Φ of 1.5% in dilute solution (5×10^{-6} M). The latter longer-wavelength emission becomes more distinct when a longer excitation wavelength is used. The emissions at 420 and 520 nm have a distinctly different excited-state lifetime (8 and 99 ns for 420 and 520 nm, respectively) (Figure 6b). As suggested by TDDFT calculations, the vertical S₁ excitation with an admixture of MLCT and LLCT transitions may be responsible for the observed lower-energy emission. This suggests that the lower-energy emission at 520 of **4**

has a similar $^3\text{MLCT}$ character as that of the mono-Ir complex **3**, while the higher-energy emission at 420 nm of **4** may have a similar Pt-perturbed $^1\text{ILCT}$ character as that of the mono-Pt complex **2**. This assignment is also in accordance with the excitation spectrum of the emission at 420 nm and 520 nm, displaying an excitation maximum at 348 and 380 nm, respectively (Figure 6c). The presence of dual emissions is likely a result of an inefficient intramolecular energy transfer process between the $^1\text{ILCT}$ and $^3\text{MLCT}$ state. A similar mechanism has been proposed for other heterodimetallic $\text{Re}^{\text{I}}\text{-Pt}^{\text{II}}$ complexes bridged by a nonconjugated aminopyridine ligand [49]. Concentration-dependent studies show that an emission band centered at 670 nm appears as the concentration was increased from 2.5×10^{-7} to 1.7×10^{-4} M (Figure 6d). This band is possibly caused by an excimeric emission due to weak intermolecular $\pi\text{-}\pi$ stackings as suggested by the above single-crystal X-ray analysis [45].

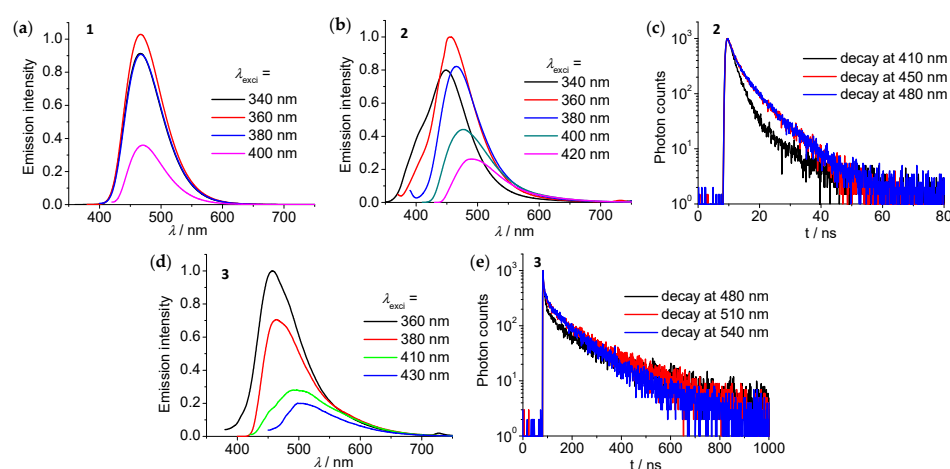


Figure 5. (a,b,d) Emission spectra of (a) **1**, (b) **2**, and (d) **3** excited at different wavelengths indicated (5×10^{-6} M in CH_3CN). (c,e) Emission decay profiles of (c) **2** and (e) **3** at different emission wavelengths indicated (5×10^{-6} M in CH_3CN). Excited at 360 nm.

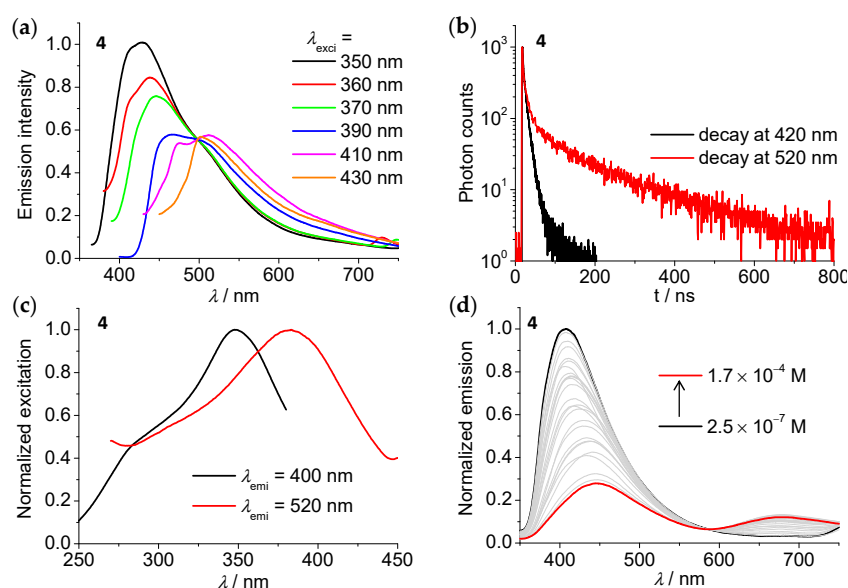


Figure 6. (a) Emission spectra of **4** excited at different wavelengths indicated (5×10^{-6} M in CH_3CN). (b) Emission decay profiles of **4** at different emission wavelengths indicated. Excited at 350 nm. (c) Excitation spectra of the emission at 400 and 520 nm of **4**. (d) Emission spectra of **4** in CH_3CN upon increasing the concentration from 2.5×10^{-7} to 1.7×10^{-4} M.

4. Conclusions

In summary, three dapz-containing monometallic and heterodimetallic complexes were designed and prepared. The two monometallic complexes **2** and **3** display a single emission band in the visible region. Interestingly, the heterodimetallic complex **4** exhibits excitation wavelength-dependent dual emissions, which are assigned to the Pt-perturbed ¹ILCT and Ir-based ³MLCT character, respectively. The inefficient energy transfer is believed for the observation of dual emissions. In contrast, most of the previously reported homo- or heterodinuclear complexes only exhibit a single emission band [50,51], consistent with Kasha's rule [52]. This suggests the unique photophysical property of metal complexes with ligand dapz. It provides important information for the future design and synthesis of dual emission photofunctional materials, which are potentially useful in the time-gated or dual-wavelength ratiometric sensing and imaging of chemical or biological systems.

Supplementary Materials: The following are available online at <https://www.mdpi.com/2073-4352/11/3/236/s1>, Tables S1 and S2: crystallographic data of complex **4**. Figure S1: The comparison of ¹H NMR spectra of **1–4**. Figure S2: Analytical HPLC of dapz and complex **4**. Figures S3–S6: ¹H- and ¹³C-NMR spectra of complex **2–4**. Figure S7: Thermogravimetric traces of complexes **3–4**. Figures S8–S9: Isodensity plots of selected frontier molecular orbitals of complex **2** and **3**. Figure S10: TDDFT results of complex **2** and **3**.

Author Contributions: Conceptualization, S.-H.W. and Y.-W.Z.; formal analysis, S.-H.W., D.-X.M., and Z.-L.G.; investigation, S.-H.W., Z.-L.G., J.-Y.S., J.M., and R.Y.; data curation, S.-H.W.; writing—original draft preparation, S.-H.W.; writing—review and editing, S.-H.W., J.-Y.S., and Y.-W.Z. All authors have written and revised the manuscript.

Funding: We thank the National Natural Science Foundation of China (22004041, 21925112, 21975264, and 21872154, 22090021), the Promotion Program for Young and Middle-aged Teacher in Science and Technology Research of Huaqiao University (ZQN-PY519), and Quanzhou City Science & Technology Program of China (2019C064R) for support with funding.

Conflicts of Interest: The authors declare no conflict of interest.

References

1. Magde, D.; Magde, M.D., Jr.; Glazer, E.C. So-called “dual emission” for 3MLCT luminescence in ruthenium complex ions: What is really happening? *Coord. Chem. Rev.* **2016**, *306*, 447–467. [CrossRef]
2. Shao, J.-Y.; Wu, S.-H.; Yang, R.; Zhong, Y.-W.; Gong, Z.-L. Dual-emissive transition-metal complexes and their applications as ratiometric photoluminescent probes. *Sci. Sin. Chim.* **2020**, *50*, 315–323. [CrossRef]
3. Keyes, T.E.; O'Connor, C.; Vos, J.G. Evidence for the presence of dual emission in a ruthenium(II) polypyridyl mixed ligand complex. *Chem. Commun.* **1998**, *1*, 889–890. [CrossRef]
4. Zambrana, J.L.; Ferloni, E.X.; Colis, J.C.; Gafney, H.D. Multiple Charge-Transfer Emissions from Different Metal-Ligand Pairs in Ruthenium Diimines. *Inorg. Chem.* **2008**, *47*, 2–4. [CrossRef]
5. Song, L.; Feng, J.; Wang, X.; Yu, J.; Hou, Y.; Xie, P.; Zhang, B.; Xiang, J.; Ai, X.; Zhang, J. Dual Emission from 3MLCT and 3ILCT Excited States in a New Ru(II) Diimine Complex. *Inorg. Chem.* **2003**, *42*, 3393–3395. [CrossRef] [PubMed]
6. Glazer, E.C.; Magde, A.D.; Tor, Y. Ruthenium Complexes That Break the Rules: Structural Features Controlling Dual Emission. *J. Am. Chem. Soc.* **2007**, *129*, 8544–8551. [CrossRef] [PubMed]
7. Blakley, R.L.; Myrick, M.L.; Dearmond, M.K. Interligand and Charge-Transfer Emission from [Ru(bpy)(HDP A)2]2+: A Dual-Emitting Ru(II) Complex. *J. Am. Chem. Soc.* **1986**, *108*, 7843–7844. [CrossRef]
8. King, K.A.; Watts, R.J. ChemInform Abstract: Dual Emission from an Ortho-Metalated Ir(III) Complex. *Cheminform* **1987**, *18*, 1589–1590. [CrossRef]
9. Gao, H.; Zhang, N.; Li, Y.; Zhao, W.; Quan, Y.; Cheng, Y.; Chen, H.Y.; Xu, J.J. Trace Ir(III) complex enhanced electrochemiluminescence of AIE-active Pdots in aqueous media. *Sci. China Chem.* **2020**, *63*, 715–721. [CrossRef]
10. Scattergood, P.A.; Ranieri, A.M.; Charalambou, L.; Comia, A.; Ross, D.A.W.; Rice, C.R.; Hardman, S.J.O.; Heully, J.L.; Dixon, I.M.; Massi, M.; et al. Unravelling the Mechanism of Excited-State Interligand Energy Transfer and the Engineering of Dual Emission in [Ir(C^N)2(N^N)]+ Complexes. *Inorg. Chem.* **2020**, *59*, 1785–1803. [CrossRef]
11. Cao, Y.; Wolf, M.O.; Patrick, B.O. Dual-Emissive Platinum(II) Metallacycles with Thiophene-Containing Bisacetylide Ligands. *Inorg. Chem.* **2016**, *55*, 8985–8993. [CrossRef] [PubMed]
12. Otto, S.; Scholz, N.; Behnke, T.; Resch-Genger, U.; Heinze, K. Thermo-Chromium: A Contactless Optical Molecular Thermometer. *Chem. Eur. J.* **2017**, *23*, 12131–12135. [CrossRef] [PubMed]

13. Cheng, Y.-M.; Yeh, Y.-S.; Ho, M.-L.; Chou, P.-T.; Chen, P.-S.; Chi, Y. Dual Room-Temperature Fluorescent and Phosphorescent Emission in 8-Quinolinolate Osmium(II) Carbonyl Complexes: Rationalization and Generalization of Intersystem Crossing Dynamics. *Inorg. Chem.* **2005**, *44*, 4594–4603. [[CrossRef](#)]
14. Li, J.; Wang, L.; Zhao, Z.; Li, X.; Yu, X.; Huo, P.; Jin, Q.; Liu, Z.; Bian, Z.; Huang, C. Two-Coordinate Copper(I)/NHC Complexes: Dual Emission Properties and Ultralong Room-Temperature Phosphorescence. *Angew. Chem. Int. Ed.* **2020**, *59*, 8210–8217. [[CrossRef](#)] [[PubMed](#)]
15. You, Y.; Han, Y.; Lee, Y.-M.; Park, S.Y.; Nam, W.; Lippard, S.J. Phosphorescent Sensor for Robust Quantification of Copper(II) Ion. *J. Am. Chem. Soc.* **2011**, *133*, 11488–11491. [[CrossRef](#)] [[PubMed](#)]
16. Liu, Y.; Guo, H.; Zhao, J. Ratiometric luminescent molecular oxygen sensors based on uni-luminophores of C Δ Pt(II)(acac) complexes that show intense visible-light absorption and balanced fluorescence/phosphorescence dual emission. *Chem. Commun.* **2011**, *47*, 11471–11473. [[CrossRef](#)] [[PubMed](#)]
17. Martin, A.; Byrne, A.; Dolan, C.; Forster, R.J.; Keyes, T.E. Solvent switchable dual emission from a bichromophoric ruthenium-BODIPY complex. *Chem. Commun.* **2015**, *51*, 15839–15841. [[CrossRef](#)]
18. Zhao, Q.; Zhou, X.; Cao, T.; Zhang, K.Y.; Yang, L.; Liu, S.; Liang, H.; Yang, H.; Li, F.; Huang, W. Fluorescent/phosphorescent dual-emissive conjugated polymer dots for hypoxia bioimaging. *Chem. Sci.* **2015**, *6*, 1825–1831. [[CrossRef](#)]
19. Zhang, K.Y.; Gao, P.; Sun, G.; Zhang, T.; Li, X.; Liu, S.; Zhao, Q.; Lo, K.K.-W.; Huang, W. Dual-Phosphorescent Iridium(III) Complexes Extending Oxygen Sensing from Hypoxia to Hyperoxia. *J. Am. Chem. Soc.* **2018**, *140*, 7827–7834. [[CrossRef](#)]
20. Gupta, S.K.; Haridas, A.; Choudhury, J. Remote Terpyridine Integrated NHC–Ir(III) Luminophores as Potential Dual-Emissive Ratiometric O₂ Probes. *Chem. Eur. J.* **2017**, *23*, 4770–4773. [[CrossRef](#)]
21. Lo, K.K.-W.; Zhang, K.Y.; Leung, S.-K.; Tang, M.-C. Exploitation of the Dual-emissive Properties of Cyclometalated Iridium(III)–Polypyridine Complexes in the Development of Luminescent Biological Probes. *Angew. Chem. Int. Ed.* **2008**, *47*, 2213–2216. [[CrossRef](#)] [[PubMed](#)]
22. Shao, J.-Y.; Wu, S.-H.; Ma, J.; Gong, Z.-L.; Sun, T.-G.; Jin, Y.; Yang, R.; Sun, B.; Zhong, Y.-W. Ratiometric detection of amyloid- β aggregation by a dual-emissive tris-heteroleptic ruthenium complex. *Chem. Commun.* **2020**, *56*, 2087–2090. [[CrossRef](#)]
23. Walker, M.G.; Ramu, V.; Meijer, A.J.H.M.; Das, A.; Thomas, J.A. A ratiometric sensor for DNA based on a dual emission Ru(dppz) light-switch complex. *Dalton Trans.* **2017**, *46*, 6079–6086. [[CrossRef](#)]
24. Hudson, Z.M.; Zhao, S.B.; Wang, R.Y.; Wang, S. Switchable Ambient-Temperature Singlet–Triplet Dual Emission in Non-conjugated Donor–Acceptor Triarylboron–Pt(II) Complexes. *Chem. Eur. J.* **2009**, *15*, 6131–6137. [[CrossRef](#)]
25. Kwak, S.W.; Choi, B.H.; Lee, J.H.; Hwang, H.; Lee, J.; Kwon, H.; Chung, Y.; Lee, K.M.; Park, M.H. Synthesis and Dual-Emission Feature of Salen-Al/Triarylborane Dyads. *Inorg. Chem.* **2017**, *56*, 6039–6043. [[CrossRef](#)]
26. Kumar, S.; Hisamatsu, Y.; Tamaki, Y.; Ishitani, O.; Aoki, S. Design and Synthesis of Heteroleptic Cyclometalated Iridium(III) Complexes Containing Quinoline-Type Ligands that Exhibit Dual Phosphorescence. *Inorg. Chem.* **2016**, *55*, 3829–3843. [[CrossRef](#)]
27. Zhang, K.Y.; Liu, H.-W.; Tang, M.-C.; Choi, A.W.-T.; Zhu, N.; Wei, X.-G.; Lau, K.-C.; Lo, K.K.-W. Dual-Emissive Cyclometalated Iridium(III) Polypyridine Complexes as Ratiometric Biological Probes and Organelle-Selective Bioimaging Reagents. *Inorg. Chem.* **2015**, *54*, 6582–6593. [[CrossRef](#)]
28. De Cola, L.; Barigelletti, F.; Balzani, V.; Belser, P.; Von Zelewsky, A.; Seel, C.; Frank, M.; Vögtle, F. Polynuclear complexes of tris(bipyridine) bridging ligands. Energy transfer from Ru-based to Os-based components. *Coord. Chem. Rev.* **1991**, *111*, 255–260. [[CrossRef](#)]
29. Aguirre-Etcheverry, P.; O’Hare, D. Electronic Communication through Unsaturated Hydrocarbon Bridges in Homobimetallic Organometallic Complexes. *Chem. Rev.* **2010**, *110*, 4839–4864. [[CrossRef](#)] [[PubMed](#)]
30. Li, G.; Zhu, D.; Wang, X.; Su, Z.; Bryce, M.R. Dinuclear metal complexes: Multifunctional properties and applications. *Chem. Soc. Rev.* **2020**, *49*, 765–838. [[CrossRef](#)] [[PubMed](#)]
31. Glazer, E.C.; Magde, D.; Tor, Y. Dual Emission from a Family of Conjugated Dinuclear Ru(II) Complexes. *J. Am. Chem. Soc.* **2005**, *127*, 4190–4192. [[CrossRef](#)]
32. Han, M.; Tian, Y.; Yuan, Z.; Zhu, L.; Ma, B. A Phosphorescent Molecular “Butterfly” that undergoes a Photoinduced Structural Change allowing Temperature Sensing and White Emission. *Angew. Chem. Int. Ed.* **2014**, *53*, 10908–10912. [[CrossRef](#)]
33. Zhou, C.; Tian, Y.; Yuan, Z.; Han, M.; Wang, J.; Zhu, L.; Tameh, M.S.; Huang, C.; Ma, B. Precise Design of Phosphorescent Molecular Butterflies with Tunable Photoinduced Structural Change and Dual Emission. *Angew. Chem. Int. Ed.* **2015**, *54*, 9591–9595. [[CrossRef](#)] [[PubMed](#)]
34. Wu, S.-H.; Shao, J.-Y.; Gong, Z.-L.; Chen, N.; Zhong, Y.-W. Tuning the dual emissions of a monoruthenium complex with a dangling coordination site by solvents, O₂, and metal ions. *Dalton Trans.* **2017**, *47*, 292–297. [[CrossRef](#)]
35. Cárdenas, D.J.; Echavarren, A.M.; De Arellano, M.C.R. Divergent Behavior of Palladium(II) and Platinum(II) in the Metalation of 1,3-Di(2-pyridyl)benzene. *Organometallics* **1999**, *18*, 3337–3341. [[CrossRef](#)]
36. Cave, G.W.V.; Alcock, A.N.W.; Rourke, J.P. High-Yield Synthesis of a C Δ N Δ C Tridentate Platinum Complex. *Organometallics* **1999**, *18*, 1801–1803. [[CrossRef](#)]
37. Constable, E.C.; Henney, P.G.; Leese, T.A.; Tocher, D.A. Cyclometallation Reactions of 6-Phenyl-2,2'-bipyridine; a Potential C,N,N-Donor Analogue of 2,2':6',2''-Terpyridine. Crystal and Molecular Structure of Dichloro-bis(6-phenyl-2,2'-bipyridine)ruthenium(II). *J. Chem. Soc. Dalton Trans.* **1990**, *2*, 443–449. [[CrossRef](#)]

38. Wu, S.H.; Burkhardt, S.E.; Yao, J.; Zhong, Y.W.; Abruña, H.D. Near-Infrared Absorbing and Emitting RuII-PtII Heterodimetallic Complexes of Dpdpz (Dpdpz = 2,3-Di(2-pyridyl)-5,6-diphenylpyrazine). *Inorg. Chem.* **2011**, *50*, 3959–3969. [[CrossRef](#)]
39. Xue, F.; Lu, Y.; Zhou, Z.; Shi, M.; Yan, Y.; Yang, H.; Yang, S. Two in One: Luminescence Imaging and 730 nm Continuous Wave Laser Driven Photodynamic Therapy of Iridium Complexes. *Organometallics* **2014**, *34*, 73–77. [[CrossRef](#)]
40. Ji, Y.; Zhang, R.; Li, Y.-J.; Li, Y.-Z.; Zuo, J.-L.; You, X.-Z. Syntheses, Structures, and Electrochemical Properties of Platinum(II) Complexes Containing Di-tert-butylbipyridine and Crown Ether Annelated Dithiolate Ligands. *Inorg. Chem.* **2007**, *46*, 866–873. [[CrossRef](#)]
41. Hua, F.; Kinayyigit, S.; Rachford, A.A.; Shikhova, E.A.; Goeb, S.; Cable, J.R.; Adams, C.J.; Kirschbaum, K.; Pinkerton, A.A.; Castellano, F.N. Luminescent Charge-Transfer Platinum(II) Metallacycle. *Inorg. Chem.* **2007**, *46*, 8771–8783. [[CrossRef](#)]
42. Ventura, B.; Barbieri, A.; Barigelletti, F.; Seneclauze, J.B.; Retailleau, P.; Ziessel, R. Trichromophoric Systems from Square-Planar Pt-Ethynylbipyridine and Octahedral Ru- and Os-Bipyridine Centers: Syntheses, Structures, Electrochemical Behavior, and Bipartition of Energy Transfer. *Inorg. Chem.* **2008**, *47*, 7048–7058. [[CrossRef](#)]
43. Wong, K.M.C.; Yam, V.W.W. Self-Assembly of Luminescent Alkynylplatinum(II) Terpyridyl Complexes: Modulation of Photophysical Properties through Aggregation Behavior. *Acc. Chem. Res.* **2011**, *44*, 424–434. [[CrossRef](#)] [[PubMed](#)]
44. Aliprandi, A.; Genovese, D.; Mauro, M.; De Cola, L. Recent Advances in Phosphorescent Pt(II) Complexes Featuring Metal-philic Interactions: Properties and Applications. *Chem. Lett.* **2015**, *44*, 1152–1169. [[CrossRef](#)]
45. Ionkin, A.S.; Marshall, W.J.; Wang, Y. Syntheses, Structural Characterization, and First Electroluminescent Properties of Monocyclometalated Platinum(II) Complexes with Greater than Classical π - π Stacking and Pt-Pt Distances. *Organometallics* **2005**, *24*, 619–627. [[CrossRef](#)]
46. Tinker, L.L.; Bernhard, S. Photon-Driven Catalytic Proton Reduction with a Robust Homoleptic Iridium(III) 6-Phenyl-2,2'-bipyridine Complex ($[\text{Ir}(\text{C}/\text{N}/\text{N})_2]^+$). *Inorg. Chem.* **2009**, *48*, 10507–10511. [[CrossRef](#)]
47. Cho, Y.J.; Kim, S.Y.; Choi, C.M.; Kim, N.J.; Kim, C.H.; Cho, D.W.; Son, H.J.; Pac, C.; Kang, S.O. Photophysics and Excited-State Properties of Cyclometalated Iridium(III)–Platinum(II) and Iridium(III)–Iridium(III) Bimetallic Complexes Bridged by Dipyrrolylpyrazine. *Inorg. Chem.* **2017**, *56*, 5305–5315. [[CrossRef](#)]
48. Tamayo, A.B.; Garon, S.; Sajoto, T.; Djurovich, P.I.; Tsyba, I.M.; Bau, R.; Thompson, M.E. Cationic Bis-cyclometalated Iridium(III) Diimine Complexes and Their Use in Efficient Blue, Green, and Red Electroluminescent Devices. *Inorg. Chem.* **2005**, *44*, 8723–8732. [[CrossRef](#)] [[PubMed](#)]
49. Kisel, K.S.; Melnikov, A.S.; Grachova, E.V.; Hirva, P.; Tunik, S.P.; Koshevoy, I.O. Linking ReI and PtII Chromophores with Aminopyridines: A Simple Route to Achieve a Complicated Photophysical Behavior. *Chem. A Eur. J.* **2017**, *23*, 11301–11311. [[CrossRef](#)] [[PubMed](#)]
50. Wong, K.M.-C.; Hui, C.-K.; Yu, K.-L.; Yam, V.W.-W. Luminescence studies of dinuclear platinum(II) alkynyl complexes and their mixed-metal platinum(II)–copper(I) and –silver(I) complexes. *Coord. Chem. Rev.* **2002**, *229*, 123–132. [[CrossRef](#)]
51. Panigati, M.; Mauro, M.; Donghi, D.; Mercandelli, P.; Mussini, P.; De Cola, L.; D'Alfonso, G. Luminescent dinuclear rhenium(I) complexes containing bridging 1,2-diazine ligands: Photophysical properties and application. *Coord. Chem. Rev.* **2012**, *256*, 1621–1643. [[CrossRef](#)]
52. Kasha, M. Characterization of electronic transitions in complex molecules. *Discuss. Faraday Soc.* **1950**, *9*, 14–19. [[CrossRef](#)]